

Polypeptoid Material as an Anchoring Material for Li–S Batteries

Deobrat Singh* and Rajeev Ahuja*

Cite This: *ACS Appl. Energy Mater.* 2021, 4, 13070–13076

Read Online

ACCESS |



Metrics & More



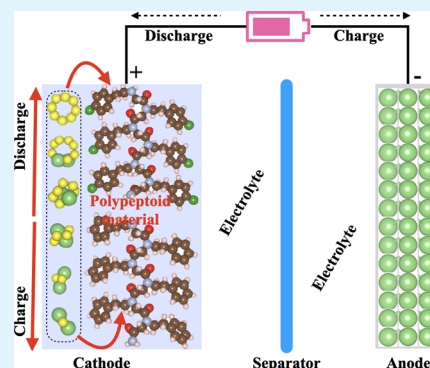
Article Recommendations



Supporting Information

ABSTRACT: Nowadays, lithium–sulfur (Li–S) batteries have attracted considerable attention as a potential candidate for next-generation rechargeable batteries due to their high theoretical specific energy and environmental friendliness. One of the main problems with Li–S batteries is that the lithium polysulfides (LiPSs) easily decompose in the electrolyte which is known as the shuttle effect. Recently, the polypeptoid nanosheet crystal structure has been experimentally synthesized which is very useful for tremendous advances in soft material imaging as well as enabling to design biomimetic nanomaterials. Due to the very interesting properties of the polypeptoid material, we have investigated the electronic structure and charge-transfer mechanism for the lithium–sulfur batteries for the cathode material. The calculated adsorption energies of LiPSs on the surface of the polypeptoid material are in the range of -4.41 to -4.64 and -0.91 eV for the sulfur clusters. Also, the adsorption energies between the interaction of LiPSs and electrolytes (DME and DOL) are 0.75 – 0.89 eV. It means that the polypeptoid material could suppress the shuttle effect of LiPSs and significantly enhance the cycling performance of Li–S batteries. From these investigated results, the polypeptoid material will be a promising anchoring material for Li–S batteries.

KEYWORDS: polypeptoid material, electronic properties, charge-transfer mechanism, binding of lithium polysulfides, Li–S battery



INTRODUCTION

With the growing population and economic development, the demand for energy technology for portable energy storage in mobile applications, for example, portable/wearable electronics and electric vehicles, has attracted great attention these days.^{1–3} Energy-storage systems based on batteries are an important technology for stabilizing renewable energy use and enhancing energy security⁴ because batteries are the integrated parts of electric vehicles, laptop computers, and cell phones.⁵ Lithium–sulfur (Li–S) batteries display better candidates for high-performance energy-storage technology because of the high theoretical specific capacity of 1675 mA h g^{-1} , a high specific energy of 2600 W h kg^{-1} among the rechargeable batteries, and also low cost, environmentally friendly, and abundance in nature of sulfur which fabricates a commercially competitive material and is suitable for large-scale production.^{6–9} However, there are some challenges that still hinder their commercial potential such as (i) a very poor conductivity of sulfur, (ii) the critical potential vanishing occurs due to the shuttle effect of the polysulfide intermediates,^{10–13} and (iii) the large volume expansion due to the density difference of lithium and sulfur.¹⁴

To overcome these issues, several cathode materials have been studied to enhance the performance of batteries.¹⁵ Until date, significant efforts have been focused to design a carbon–sulfur composite cathode to reduce the shuttle effect, but it remains challenging to suppress the migration and dissolution of polysulfides in the organic electrolyte.^{11,16–22} Recently, the significant modification of separators using different types of

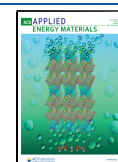
porous materials such as porous carbon^{23,24} and other types of porous materials, conducting polymers,^{25,26} metal–organic frameworks (MOFs),²⁷ or 2D materials^{28,29} has been displayed as an effective way to improve the cycle performance of Li–S batteries, in which the modified separator can impressively suppress polysulfide migration to the anodes.³ The reported literature suggests that the characteristics of the materials added such as the separator, electrolyte, interlayer, anode, and cathode in the separators are important factors in deciding the performance of the battery.

It was reported that the poly(leucine–lysine)-based peptide significantly suppresses the sulfur loss in the electrolyte and also proposes that it is very useful for potential applications in Li–S batteries as a coating material.³⁰ The polypeptoid material contains carbon (C), oxygen (O), and nitrogen (N) atoms and benzene groups. Due to the effect of electronegativity, the atoms generate polar and nonpolar bonds between C–O and C–N. Also, the benzene ring has a large electron cloud density that appears from a conjugated π -orbital electron which interacts with LiPSs and it could be the most active interaction site to inhibit the loss of polysulfides. Therefore, such types of materials

Received: September 1, 2021

Accepted: October 18, 2021

Published: October 29, 2021



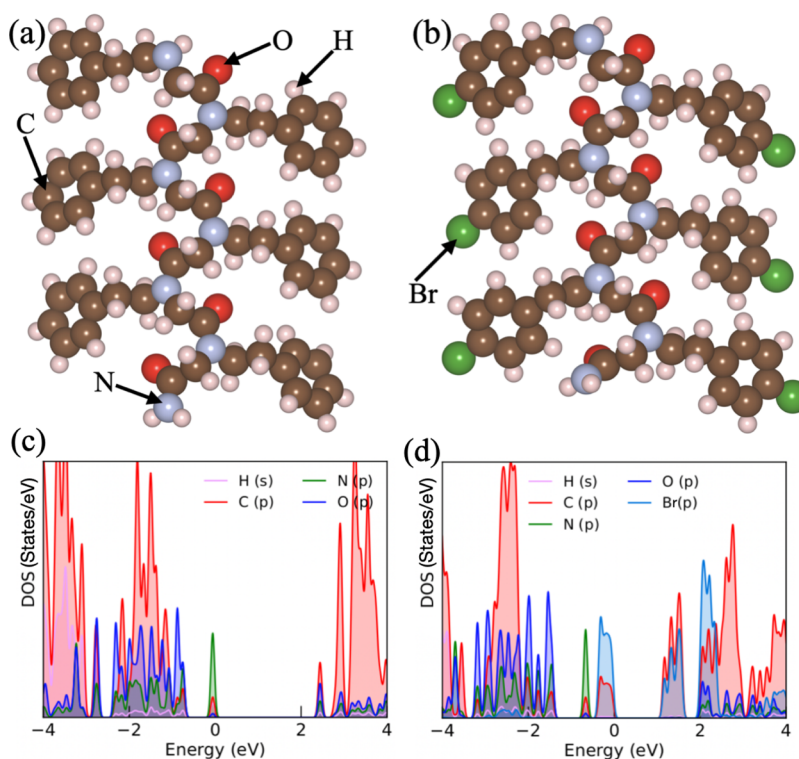


Figure 1. Chemical structures of (a) Nte4-Npe6 and (b) Nte4-N4Brpe6 polypeptoid materials. The carbon, oxygen, nitrogen, hydrogen, and bromine atoms are represented by brown, red, blue gray, light pink, and green, respectively. Projected density of states of (c) Nte4-Npe6 and (d) Nte4-N4Brpe6 polypeptoid materials.

could be better candidates for Li–S batteries. In addition, a 2D polypeptoid nanosheet has been recently successfully synthesized.³¹ Motivated by these abovementioned studies, we have investigated the thermal stability at 300 K using *ab initio* molecular dynamics (AIMD) simulations and it maintained the structural configuration for 10 ps and no breaking of bonds between the atoms confirmed the structural stability. In the present work, we have proposed the newly synthesized organic polypeptoid material structure for Li–S batteries for cathode materials which are investigated by density functional theory calculations. The physical and chemical interactions of Li_2S_x ($x = 1, 2, 4, 6$, and 8) and S_8 clusters with the polypeptoid material are investigated. Furthermore, we compute the nature of bonding and charge transfer between Li_2S_x and polypeptoid material. We have also investigated the diffusion and decomposition energy barrier of Li_2S which is lower than most of the materials used in Li–S batteries. We found that these finding results such as strong binding energy between Li_2S_x , the lower energy barrier of the polypeptoid material ensuring excellent materials for Li–S batteries.³²

COMPUTATIONAL METHODS

The electronic structure calculations are based on the DFT approach using VASP code.^{33–35} To describe the core electrons and electron–ion interactions, the projector-augmented-wave pseudopotentials were used.³⁶ The exchange–correlation energy was described via the Perdew, Burke and Ernzerhof functional within generalized gradient approximation.³⁷ The energy cutoff of 500 eV has been used for the plane-wave basis set, and Γ -point sampling was used. To prevent the physical interaction between the periodic images, we have taken 15 Å in each direction. We have used the DFT-D3 procedure in order to include the van der Waals interaction.^{38,39} For the chemical structure visualizations and plots, we have used VESTA software.⁴⁰ During the calculations for self-consistent and electronic density of states, we have

used the Gaussian broadening of 0.06 eV. For structural optimizations, a combination of conjugate-gradient algorithm and a quasi-Newton force minimization was used.⁴¹ During the calculations, all the atoms were allowed to fully relax until forces acting on atoms were less than 0.005 eV/Å. To determine the energy barrier, we have used the climbing image nudged elastic band method that is implemented in the VASP-VTST tools.^{42,43} We have used the AIMD simulations to check the thermal stability of the polypeptoid material at room temperature. The NVT ensemble has been used for 10 ps with a time step of 2 fs, and the considered temperature was controlled by the Nosé–Hoover method.⁴⁴ The Bader charge analysis⁴⁵ has been used to calculate the charge transfer between the LiPS species and substrate.

RESULTS AND DISCUSSION

Structural and Electronic Properties. The optimized structures of polypeptoid material with different configurations, that is, Nte4-Npe6 (conf.-1) and Nte4-N4Brpe6 with Br atoms (conf.-2), are shown in Figure 1. Here, poly(*N*-2-(2-methoxyethoxy)ethoxy)ethylglycine is represented by Nte and *N*-(2-phenylethyl)glycine is represented by Npe. The considered polypeptoids Nte4-Npe6 and Nte4-N4Brpe6 are almost similar, but in the case of polypeptoids Nte4-Npe6, each benzene ring is attached by one hydrogen (H) atom, while in the case of polypeptoids Nte4-N4Brpe6 configuration, each benzene ring is connected by bromine (Br) atoms. Here, the electronegativity of the Br atom is larger than the H atom; therefore, it could affect the physical and chemical properties of materials. The optimized bond lengths between C–C, C–O, C–N, C–H, N–H, and C–Br are 1.40 Å in a hexagonal ring (1.54 Å in other places), 1.23 and 1.37 Å when C is attached with an O atom (1.45 Å when C is attached with a H atom), and 1.10, 1.01, and 1.53 Å in conf.-1 and conf.-2 which is well consistent with the previous literature.³¹ Moreover, we have investigated the AIMD simulations to check the thermal stability of the

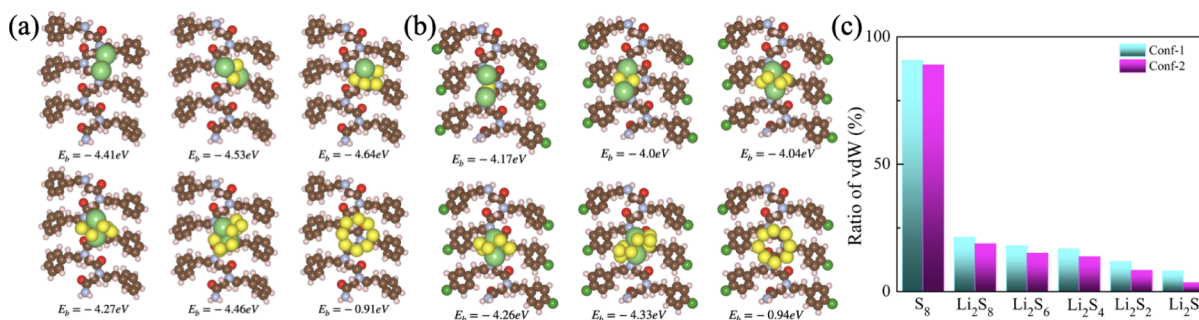


Figure 2. Binding strength of Li–S composites on the surface of the polypeptoid material of (a) conf.-1 and (b) conf.-2. (c) Ratio for vdW interaction for the polypeptoid material of conf.-1 and conf.-2 at different lithiation stages.

polypeptoid material. The final structures of polypeptoid material are depicted in Figures S1 and S2 (see the [Supporting Information](#)). The AIMD simulations have been performed at room temperature for 10 ps and it was seen that there is no structure distortion and no bond breaking inside the polypeptoid material. It means that the polypeptoid material has good thermal stability.

Furthermore, to better understand the electronic properties of the polypeptoid material, we have investigated the density of states (DOS) (see [Figure 1c,d](#)). From the DOS, the highest-occupied molecular orbital (HOMO) and lowest-unoccupied molecular orbital (LUMO) are well-separated, which means that both configurations displayed the semiconducting behavior. The HOMO–LUMO gap in the case of conf.-1 and conf.-2 is 2.47 and 1.25 eV, respectively. Also, the HOMO is mostly originated by N p-orbitals, while the LUMO is mostly contributed by p-orbitals of C and O atoms. It means that these states are dominating near the Fermi level (see [Figure 2a](#)), in conf.-1. While in the case of conf.-2, the HOMO is formed by p-orbitals of both Br and a less part originated from C p-orbitals, and the LUMO is mostly originated by p-orbitals of Br and C atoms. Furthermore, from the Bader charge analysis, the atomic charges are arranged as per requirement. The N atom gains 1.10 e, the C atom donates 0.14 e, O atoms gain 1.13 e, and the H atom donates 0.06 e to the surrounding atoms in conf.-1. Similarly, in the case of conf.-2, the N, C, O, H, and Br atoms 1.13 e (gains), 0.11 e (donates), 1.13 e (gains), 0.07 e (donates), and 0.71 e (donates) to the surrounding atoms, respectively. More importantly, due to the presence of oxygen and nitrogen atoms in the middle part of the polypeptoid material, therefore, it would enhance the performance of the Li–S battery by anchoring a polar lithium polysulfide intermediate.

Adsorption and Charge-Transfer Mechanism. One of the main difficulties with Li–S batteries is that the intermediate LiPSs easily dissolve into the electrolyte which reduces the performance of the Li–S batteries. To prevent the shuttle effect, that is, dissolution of LiPS species into the electrolyte, it is necessary that the binding energy of LiPS species with the anchoring material should be larger than that of the organic electrolyte molecules. The optimized molecular structures of LiPSs and organic electrolytes are presented in Figure S3 (see the [Supporting Information](#)). The binding energy (E_b) of LiPSs on the surface of the polypeptoid material is given as

$$E_b = E_{(\text{substrate} + \text{LiPSs})} - E_{\text{substrate}} - E_{\text{LiPSs}} \quad (1)$$

where $E_{(\text{substrate} + \text{LiPSs})}$, $E_{\text{substrate}}$, and E_{LiPSs} represent the total energy of the substrate with LiPSs, substrate, and isolated LiPS species, respectively. Using [eq 1](#), we have investigated the

binding energy of LiPSs and S_8 species on the polypeptoid material. During the charging and discharging process, S-containing clusters such as Li_2S_x (i.e., $x = 1, 2, 4, 6$, and 8) and S_8 are generated. Initially, we have considered different orientations and different positions in which [Figure 2](#) displayed the fully optimized with the lowest energy configuration for both cases. Particularly, for these types of adsorption systems, previous investigations have demonstrated that the bond appears through the coordinated effect of vdW and covalent bonding.⁴⁶ First, we have systematically investigated the ratio of vdW interactions to see the strength of chemical and physical adsorption influence of anchoring effects. Here, the vdW interaction ratio is as follows

$$R_{\text{vdW}}(\%) = \left(\frac{E_b^{\text{PBE+vdW}} - E_b^{\text{PBE}}}{E_b^{\text{PBE+vdW}}} \right) 100 \quad (2)$$

where E_b^{PBE} and $E_b^{\text{PBE+vdW}}$ are the terms of E_b which comes from the standard PBE functional and PBE functional with the addition of the vdW term. [Figure 2](#) displays the strength of vdW interactions provided significantly and clearly for two different configurations of the electrodes. The chemical and vdW interactions play a significant role in the case of de-lithiation from Li_2S to Li_2S_8 , in which the strength of the vdW interaction to the binding energies conclusively increases and reaches up to 21.35 and 19% in conf.-1 and conf.-2, respectively. While the ratio of the vdW interaction for species S_8 has almost reached 90% (see [Figure 2c](#)). All the lowest adsorption configurations with the top view of Li_2S_x and S_8 species are depicted in [Figure 2a,b](#) for conf.-1 and conf.-2, respectively. Additionally, the side view of these two configurations is presented in Figures S4 and S5 (see the [Supporting Information](#)). It was seen that the S_8 species lies parallel to the top of the polypeptoid sheet and the vertical distance of 2.99 Å/3.29 Å for conf.-1/conf.-2 of the polypeptoid material, respectively. From the Bader charge analysis, a relatively small amount of charge transfer (0.074 e/0.02 e for conf.-1/conf.-2) has been found. The less amount of charge transfer indicates the weak chemical interaction between the S_8 species and polypeptoid surface which is also confirmed by the relatively lower binding strength (see [Figure 2a,b](#)).

From [Figure 2a,b](#), we can clearly see that the positions and orientations of adsorbed species, that is, LiPSs and S_8 clusters on the surface of the polypeptoid, are slightly different. Because the electronegativity of the Br atom is larger than the H atom attached with benzene rings in conf.-1 and conf.-2, therefore, it affected the physical/chemical interactions of adsorbed species on these two configurations. [Figure 2a](#) shows that the other adsorption configurations in which Li_2S_8 species prefers relatively lying near to the substrate and both Li atoms lie toward the polypeptoid surface in both configurations. Similar to

Li_2S_8 species, the Li_2S_6 species also prefer the same orientation, and the vertical height between the species and substrate is almost equal. While both Li atoms are parallel to the surface in the case of conf.-1 and conf.-2, the one Li atom is slightly lower than other Li atoms in the adsorbed Li_2S_6 species on the surface of the polypeptoid. In contrast, the lower-order species Li_2S_x ($x = 1, 2$, and 4) prefer to form chemical bonding of one Li atom to N atom from the polypeptoid surface in the case of conf.-1, whereas one Li atom of Li_2S_2 species forms chemical bonding to the polypeptoid surface, and the other two only have a chemical interaction with the substrate. Additionally, the lower-order species Li_2S_x ($x = 1, 2$, and 4) have relatively lower vertical height between the species and substrate, and also, it has higher charge transfer between them (see Table 1). As the discharge process

Table 1. Optimized Structural Parameters Such as Vertical Distance between the Polypeptoid Material and LiPS Species^a

		S_8	Li_2S_8	Li_2S_6	Li_2S_4	Li_2S_2	Li_2S
conf-1	$d_{\text{sheet-LiPSs}}$	2.99	2.61	2.66	1.95	1.79	1.90
	Q	0.07	0.13	0.21	0.31	0.54	0.61
conf-2	$d_{\text{sheet-LiPSs}}$	3.29	2.65	2.85	3.02	2.07	2.17
	Q	0.02	0.09	0.18	0.28	0.45	0.48

^aCharge-transfer values between the polypeptoid material and LiPS species. The positive values of charge represent the transfer of LiPS species to the polypeptoid surface.

proceeds, more and more electrons are transferred from the LiPSs species to the polypeptoid substrate, which shows that the strength of chemical interactions increases during the lithiation process. The positive values of the charge transfer display the polypeptoid that gains electrons from the LiPSs and S_8 species, as presented in Table 1. In both cases conf.-1 and conf.-2, electrons are transferred from LiPSs and S_8 species to the polypeptoid surface. It was seen that the charge-transfer values in

conf.-1 are slightly larger than those of conf.-2, which reflects the binding strength between the LiPSs and S_8 species and polypeptoid surface. Also, a less amount of charge transfer refers to the relatively low chemical interactions. Apart from this, the lower-order S-containing species in LiPSs have higher charge transfer as compared to the higher-order S-containing species in LiPSs (see Table 1). From these investigations, we can see that when Br atoms are attached with each benzene ring (conf.-2), then the binding strength of LiPSs is slightly decreased as compared to H-connected benzene rings (conf.-1). Generally, Li_2S_x clusters are also nicely maintained during adsorption, indicating that the polypeptoid sheet is a suitable candidate for Li-S batteries as a cathode anchoring material.

Furthermore, to analyze the anchoring performance of the polypeptoid material, we have systematically investigated the binding energies of LiPSs on the surface of the polypeptoid material and the corresponding results are presented in Figure 3a. It was reported that the suitable solvent for the Li-S cell electrolytes is limited such as dimethyl ether (DME) and 1,3-dioxolane (DOL) used commonly.^{47,48} It was seen that both DME and DOL electrolytes lead to synergistic effects on the retention capacity and specific capacity of sulfur as compared to the solvent alone.⁴⁹ Because of this, we have investigated the binding energies of commonly used electrolytes (DOL and DME) with LiPS species. The considered electrolyte is the liquid phase in which S_8 species is not soluble.⁵⁰ The fully optimized structures of isolated LiPSs, as well as S_8 and electrolyte (DOL and DME), are presented in Figure S3 in the Supporting Information. Also, the lowest energy configuration structures of LiPSs with an electrolyte (DOL and DME) are presented in Figure S6 in the Supporting Information. From Figure 3a, we can see that the polypeptoid material shows better performance for all lithium polysulfides.

Due to the presence of only S atoms in S_8 species, it has no polarity. Therefore, the E_b of S_8 for both the configurations is nearly equal and relatively very less as compared to other

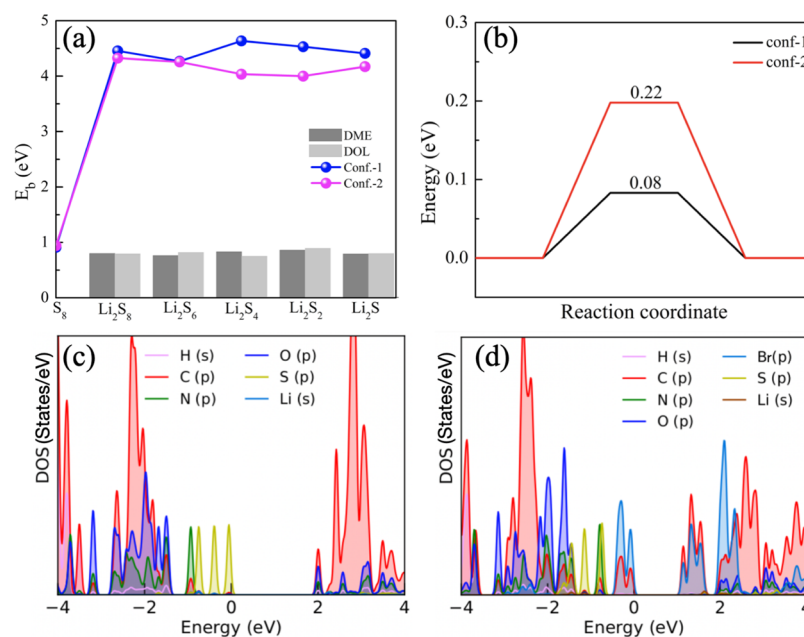


Figure 3. (a) Binding strength of LiPSs and S_8 clusters on the surface of the polypeptoid material and the corresponding binding energies of LiPSs with electrolytes for comparison. (b) Calculated energy barriers of Li_2S diffusion on the surface of the polypeptoid material. (c,d) Projected DOS of polypeptoid material.

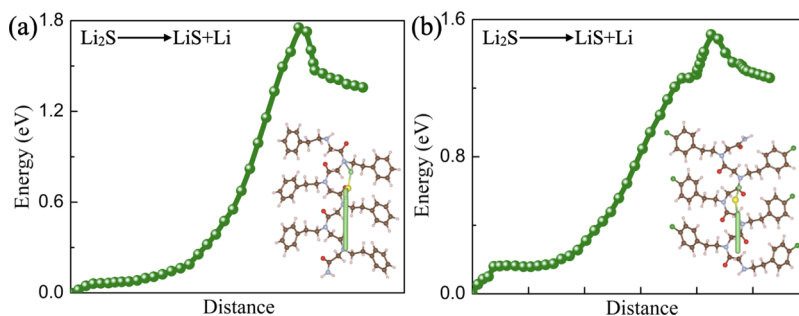
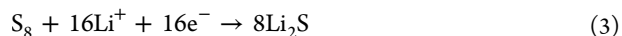


Figure 4. Diffusion process of decomposition of Li_2S species and energy curve on the surface of the polypeptoid material for (a) conf.-1 and (b) conf.-2.

adsorbed species.⁵¹ Also, due to no polarity in S_8 species trying to lie in a parallel orientation to the surface, it has a very small charge transfer between them. Whenever the top surface contains O, F, Cl, and N atoms (i.e., generally higher electronegativity as compared to the rest of the atoms) in the materials, then such types of materials could capture more effectively the polar LiPS species than the rest of the layered materials.^{50,51} Due to the presence of O and N at the middle of the Nte4-Npe6 and Nte4-N4Brpe6 polypeptoid material, it has more strength to capture the polar LiPS species. The calculated binding energies of Nte4-Npe6 and Nte4-N4Brpe6 polypeptoid material are mentioned (see Figure 3a). The E_b is varying from 0.91 to 4.64 and 0.94 to 4.33 eV for conf.-1 and conf.-2, respectively, and 0.75–0.89 eV for both electrolytes. The optimized interactions between the electrolytes and LiPS species are presented in Figure S6 (see the Supporting Information). The binding energies between electrolytes and LiPS species are lower than the corresponding binding energy values between the polypeptoid material and LiPS species which suggest that the LiPS species strongly absorb on the polypeptoid material rather than dissolve into the electrolytes. Furthermore, the binding energies over the polypeptoid material are stronger than most of the studied 2D-layered materials.^{51–53} It means that the polypeptoid material is firmly anchored to all sulfur-containing species. From the abovementioned descriptions, both configurations of the polypeptoid material have a stronger affinity to bind the sulfur-containing clusters that suppress the shuttle effect which as a result improves the overall performance of Li–S batteries.

Also for anchoring material, the surface diffusion properties are an important parameter that will be affected by the growth and distribution of sulfide species at the electrode, whereby the optimized balance between the adsorption of sulfur-containing clusters and surface diffusion properties display a significant role in Li–S battery performance.⁵⁴ During discharging case, the cathode of Li–S batteries is defined as



That is why we have considered Li_2S species to compute the energy barrier toward the particular diffusion pathway for conf.-1 and conf.-2. Initially, we have optimized the vertical distance to get the minimum energy configuration of polypeptoid materials with Li_2S species. Also, we have checked the two most favorable positions of Li_2S species with minimum energy configurations; after that, we have decided the diffusion direction to get the activation energy. The activation energy is calculated by the climbing image-nudged elastic band method. Figure 3b displays the diffusion energy barriers of conf.-1 and conf.-2 of the polypeptoid material and the corresponding energy barriers are

0.08 and 0.22 eV, respectively. From the energy barrier, conf.-1 has a lower value for the diffusion of Li_2S species on the surface of the polypeptoid material. From the Arrhenius equation, the diffusion constant (D) is directly proportional to the $\exp(-E_a/k_B T)$.⁵⁵ In this equation, E_a , k_B , and T represent the energy barrier, Boltzmann's constant, and absolute temperature, respectively. Here, we have estimated the diffusion constant (D) of Li_2S at room temperature which is $\sim 10^6$ times faster than nonconductive metal oxide (i.e., energy barrier lies between 0.45 and 1.22 eV)⁵⁴ and 22 times faster than conductive layered materials (i.e., their energy barrier lies between 0.22 and 0.16 eV).^{50,55} It means that when it will be used as a cathode material in Li–S batteries, then we expect that the polypeptoid material will give good cycling performance.

The good electrical conductivity of sulfur cathode host materials is also affecting the operability and performance of the Li–S batteries which is essential to significantly govern the performance of Li–S batteries. Therefore, to understand the electrical conductivity, the DOS of Li_2S adsorbed on the surface of the polypeptoid material has been calculated. Figure 3c,d represents the PDOS for conf.-1 and conf.-2 of the polypeptoid material after the adsorption of Li_2S species. From Figure 3c,d, the significantly enhanced electronic states near the F_F are observed. Here, we found that the Li_2S cluster adsorbed on polypeptoid materials and then it reduces the HOMO–LUMO gap from 2.47 to 1.99 eV for conf.-1 while 1.25 to 1.13 eV for conf.-2. During the adsorption of Li_2S species on the surface of polypeptoid materials, the Li_2S species transfer 0.61 e and 0.48 e to the surface in the case of conf.-1 and conf.-2, respectively, which is confirmed by Bader charge analysis (see Table 1). It means that the S atom from Li_2S species is strongly hybridized with C, N, and O atoms from the surface in both configurations. Also, it was seen that the Fermi level is shifted because the electronic states come from S orbitals, that is, HOMO is mainly made by S orbitals from Li_2S species in the case of conf.-1. However, in the case of conf.-2, some of the electronic states appear around -1 eV in the HOMO due to the significant hybridization of the orbitals of Li_2S species and surface atoms. These hybridizations are responsible for enhancing the electrical conductivity in the considered materials. Due to the presence of an electronic state near the Fermi level, it enhances the electrical conductivity of the polypeptoid material after the adsorption of the Li_2S cluster that will significantly enhance the performance of Li–S batteries.

It is well-known that the low-order sulfur-containing cluster Li_2S begins to decompose and oxidize to high-order sulfur clusters and finally form S_8 clusters during the charging process of Li–S batteries. It is also well-known that catalysis of the decomposition of Li_2S clusters near the surface of the substrate is a vital step to appreciate high capacity, as well as Coulombic

efficiency.⁵⁶ Apart from this, the energy barrier of the decomposition Li_2S species qualitatively agrees by measurement of voltage magnitude in experiments.⁵⁶ In the present work, the decomposition process of Li_2S species from Li_2S molecules into LiS species, single Li^+ , and single electron, that is, $\text{Li}_2\text{S} \rightarrow \text{LiS} + \text{Li}^+ + \text{e}^-$, has been considered. During the reaction, Li^+ moves away from the S atom in the Li_2S molecule, by the breaking of the Li–S bond. Figure 4 shows the decomposition energy barrier of Li_2S species on the surface of both the configuration of the polypeptoid material. The calculated energy barrier is found to be 1.51 eV in conf.-2 which is lower than the graphene.⁵⁶ It means that the polypeptoid material is a superior candidate for improving the performance of Li–S batteries.

CONCLUSIONS

We have systematically investigated the polypeptoid material as an anchoring material for Li–S batteries. From the first-principles calculations, we have calculated the binding energy of LiPS species on the surface of the polypeptoid material which are higher than the binding energy of the electrolytes with LiPS species. Additionally, the diffusion energy barrier of Li_2S for conf.-1 is lower than the conf.-2 of the polypeptoid material and the decomposition energy barrier is relatively low as compared to most of the materials used in Li–S batteries. These findings results suggest that the polypeptoid material can display strong binding energy and fast diffusion, confirming the rapid discharge and charging processes for LiS batteries. The present work demonstrates that the polypeptoid material will be a good candidate for the sulfur cathode.

ASSOCIATED CONTENT

Supporting Information

The Supporting Information is available free of charge at <https://pubs.acs.org/doi/10.1021/acsaem.1c02712>.

AIMD simulated structures of Nte4-Npe6 and Nte4-N4Brpe6 polypeptoid material, fully optimized structures of LiPS s, S_8 species and organic electrolyte, side view of adsorbate species on the polypeptoid surface, and lowest energy configurations of LiPS species with organic electrolytes DOL and DME (PDF)

AUTHOR INFORMATION

Corresponding Authors

Deobrat Singh – Condensed Matter Theory Group, Materials Theory Division, Department of Physics and Astronomy, Uppsala University, 75120 Uppsala, Sweden; orcid.org/0000-0001-7246-8743; Email: deobrat.singh@physics.uu.se

Rajeev Ahuja – Condensed Matter Theory Group, Materials Theory Division, Department of Physics and Astronomy, Uppsala University, 75120 Uppsala, Sweden; Department of Physics, Indian Institute of Technology Ropar, Rupnagar 140001 Punjab, India; orcid.org/0000-0003-1231-9994; Email: rajeev.ahuja@physics.uu.se

Complete contact information is available at: <https://pubs.acs.org/doi/10.1021/acsaem.1c02712>

Notes

The authors declare no competing financial interest.

ACKNOWLEDGMENTS

D.S. and R.A. thank the Swedish Research Council (VR-2016-06014 and VR2020-04410) and J. Gust. Richert stiftelse, Sweden (2021-00665) for financial support. D.S. and R.A. gratefully acknowledge computational resources from the Swedish National Infrastructure for Computing SNIC and HPC2N.

REFERENCES

- (1) Liu, B.; Bo, R.; Taheri, M.; Di Bernardo, I.; Motta, N.; Chen, H.; Tsuzuki, T.; Yu, G.; Tricoli, A. Metal-Organic Frameworks/Conducting Polymer Hydrogel Integrated Three-Dimensional Free-Standing Monoliths as Ultrahigh Loading Li-S Battery Electrodes. *Nano Lett.* **2019**, *19*, 4391–4399.
- (2) Bai, L.; Chao, D.; Xing, P.; Tou, L. J.; Chen, Z.; Jana, A.; Shen, Z. X.; Zhao, Y. Refined Sulfur Nanoparticles Immobilized in Metal-Organic Polyhedron as Stable Cathodes for Li-S Battery. *ACS Appl. Mater. Interfaces* **2016**, *8*, 14328–14333.
- (3) Li, M.; Wan, Y.; Huang, J.-K.; Assen, A. H.; Hsiung, C.-E.; Jiang, H.; Han, Y.; Eddaoudi, M.; Lai, Z.; Ming, J.; Li, L.-J. Metal-Organic Framework-Based Separators for Enhancing Li-S Battery Stability: Mechanism of Mitigating Polysulfide Diffusion. *ACS Energy Lett.* **2017**, *2*, 2362–2367.
- (4) Gao, G.; Sun, X.; Wang, L.-W. An inverse vulcanized conductive polymer for Li-S battery cathodes. *J. Mater. Chem. A* **2020**, *8*, 21711–21720.
- (5) Zubi, G.; Dufo-López, R.; Carvalho, M.; Pasaoglu, G. The lithium-ion battery: State of the art and future perspectives. *Renewable Sustainable Energy Rev.* **2018**, *89*, 292–308.
- (6) Wu, H. B.; Wei, S.; Zhang, L.; Xu, R.; Hng, H. H.; Lou, X. W. D. Embedding Sulfur in MOF-Derived Microporous Carbon Polyhedrons for Lithium-Sulfur Batteries. *Chem.—Eur. J.* **2013**, *19*, 10804–10808.
- (7) Bai, L.; Tu, B.; Qi, Y.; Gao, Q.; Liu, D.; Liu, Z.; Zhao, L.; Li, Q.; Zhao, Y. Enhanced performance in gas adsorption and Li ion batteries by docking Li^+ in a crown ether-based metal-organic framework. *Chem. Commun.* **2016**, *52*, 3003–3006.
- (8) Yang, X.; Li, X.; Adair, K.; Zhang, H.; Sun, X. Structural Design of Lithium-Sulfur Batteries: From Fundamental Research to Practical Application. *Electrochem. Energy Rev.* **2018**, *1*, 239–293.
- (9) Zhang, Z.; Kong, L.-L.; Liu, S.; Li, G.-R.; Gao, X.-P. A High-Efficiency Sulfur/Carbon Composite Based on 3D Graphene Nanosheet@Carbon Nanotube Matrix as Cathode for Lithium-Sulfur Battery. *Adv. Energy Mater.* **2017**, *7*, 1602543.
- (10) Mikhaylik, Y. V.; Akridge, J. R. Polysulfide shuttle study in the Li/S battery system. *J. Electrochem. Soc.* **2004**, *151*, A1969.
- (11) Zheng, G.; Yang, Y.; Cha, J. J.; Hong, S. S.; Cui, Y. Hollow carbon nanofiber-encapsulated sulfur cathodes for high specific capacity rechargeable lithium batteries. *Nano Lett.* **2011**, *11*, 4462–4467.
- (12) Kolosnitsyn, V. S.; Karaseva, E. V. Lithium-sulfur batteries: Problems and solutions. *Russ. J. Electrochem.* **2008**, *44*, 506–509.
- (13) Lin, Z.; Liu, Z.; Dudney, N. J.; Liang, C. Lithium Superionic Sulfide Cathode for All-Solid Lithium-Sulfur Batteries. *ACS Nano* **2013**, *7*, 2829–2833.
- (14) Wang, J.; Si, L.; Wei, Q.; Hong, X.; Lin, L.; Li, X.; Chen, J.; Wen, P.; Cai, Y. An imine-linked covalent organic framework as the host material for sulfur loading in lithium-sulfur batteries. *J. Energy Chem.* **2019**, *28*, 54–60.
- (15) Baumann, A. E.; Burns, D. A.; Díaz, J. C.; Thoi, V. S. Lithiated Defect Sites in Zr Metal-Organic Framework for Enhanced Sulfur Utilization in Li-S Batteries. *ACS Appl. Mater. Interfaces* **2018**, *11*, 2159–2167.
- (16) Wang, H.; Yang, Y.; Liang, Y.; Robinson, J. T.; Li, Y.; Jackson, A.; Cui, Y.; Dai, H. Graphene-Wrapped Sulfur Particles as a Rechargeable Lithium-Sulfur Battery Cathode Material with High Capacity and Cycling Stability. *Nano Lett.* **2011**, *11*, 2644–2647.
- (17) Chen, S.-R.; Zhai, Y.-P.; Xu, G.-L.; Jiang, Y.-X.; Zhao, D.-Y.; Li, J.-T.; Huang, L.; Sun, S.-G. Ordered mesoporous carbon/sulfur

nanocomposite of high performances as cathode for lithium-sulfur battery. *Electrochim. Acta* **2011**, *56*, 9549–9555.

(18) Navaneedhakrishnan, J.; Shen, J.; Moganty, S. S.; Corona, A.; Archer, L. Porous Hollow Carbon Sulfur Composites for High Power Lithium-Sulfur Batteries. *ECS Meeting Abstracts*; IOP Publishing, 2011; Vo. 341.

(19) Zheng, J.; Guo, G.; Li, H.; Wang, L.; Wang, B.; Yu, H.; Yan, Y.; Yang, D.; Dong, A. Elaborately Designed Micro-Mesoporous Graphitic Carbon Spheres as Efficient Polysulfide Reservoir for Lithium-Sulfur Batteries. *ACS Energy Lett.* **2017**, *2*, 1105–1114.

(20) Luo, L.; Manthiram, A. Rational Design of High-Loading Sulfur Cathodes with a Poached-Egg-Shaped Architecture for Long-Cycle Lithium-Sulfur Batteries. *ACS Energy Lett.* **2017**, *2*, 2205–2211.

(21) Kim, H. M.; Sun, H.-H.; Belharouak, I.; Manthiram, A.; Sun, Y.-K. An Alternative Approach to Enhance the Performance of High Sulfur-Loading Electrodes for Li-S Batteries. *ACS Energy Lett.* **2016**, *1*, 136–141.

(22) Je, S. H.; Hwang, T. H.; Talapaneni, S. N.; Buyukcakir, O.; Kim, H. J.; Yu, J.-S.; Woo, S.-G.; Jang, M. C.; Son, B. K.; Coskun, A.; Choi, J. W. Rational Sulfur Cathode Design for Lithium-Sulfur Batteries: Sulfur-Embedded Benzoxazine Polymers. *ACS Energy Lett.* **2016**, *1*, 566–572.

(23) Zhang, X.; Cheng, X.; Zhang, Q. Nanostructured energy materials for electrochemical energy conversion and storage: a review. *J. Energy Chem.* **2016**, *25*, 967–984.

(24) Peng, H.-J.; Huang, J.-Q.; Cheng, X.-B.; Zhang, Q. Lithium-Sulfur Batteries: Review on High-Loading and High-Energy Lithium-Sulfur Batteries (Adv. Energy Mater. 24/2017). *Adv. Energy Mater.* **2017**, *7*, 1770141.

(25) Wu, F.; Chen, J.; Chen, R.; Wu, S.; Li, L.; Chen, S.; Zhao, T. Sulfur/polythiophene with a core/shell structure: synthesis and electrochemical properties of the cathode for rechargeable lithium batteries. *J. Phys. Chem. C* **2011**, *115*, 6057–6063.

(26) Li, G.-C.; Li, G.-R.; Ye, S.-H.; Gao, X.-P. A polyaniline-coated sulfur/carbon composite with an enhanced high-rate capability as a cathode material for lithium/sulfur batteries. *Adv. Energy Mater.* **2012**, *2*, 1238–1245.

(27) Xi, K.; Cao, S.; Peng, X.; Ducati, C.; Vasant Kumar, R.; Cheetham, A. K. Carbon with hierarchical pores from carbonized metal-organic frameworks for lithium sulphur batteries. *Chem. Commun.* **2013**, *49*, 2192–2194.

(28) Ghazi, Z. A.; He, X.; Khattak, A. M.; Khan, N. A.; Liang, B.; Iqbal, A.; Wang, J.; Sin, H.; Li, L.; Tang, Z. MoS₂/Celgard Separator as Efficient Polysulfide Barrier for Long-Life Lithium-Sulfur Batteries. *Adv. Mater.* **2017**, *29*, 1606817.

(29) Sun, J.; Sun, Y.; Pasta, M.; Zhou, G.; Li, Y.; Liu, W.; Xiong, F.; Cui, Y. Entrapment of Polysulfides by a Black-Phosphorus-Modified Separator for Lithium-Sulfur Batteries. *Adv. Mater.* **2016**, *28*, 9797–9803.

(30) Jewel, Y.; Yoo, K.; Liu, J.; Dutta, P. Self-assembled peptides for coating of active sulfur nanoparticles in lithium-sulfur battery. *J. Nanoparticle Res.* **2016**, *18*, 54.

(31) Xuan, S.; Jiang, X.; Spencer, R. K.; Li, N. K.; Prendergast, D.; Balsara, N. P.; Zuckermann, R. N. Atomic-level engineering and imaging of polypeptoid crystal lattices. *Proc. Natl. Acad. Sci.* **2019**, *116*, 22491–22499.

(32) Zhang, J.; Yang, G.; Tian, J.; Wang, Y.; Ma, D. Modulating electronic and optical properties of black phosphorus carbide monolayers by molecular doping. *Appl. Surf. Sci.* **2018**, *448*, 270–280.

(33) Kresse, G.; Joubert, D. From ultrasoft pseudopotentials to the projector augmented-wave method. *Phys. Rev. B: Condens. Matter Mater. Phys.* **1999**, *59*, 1758.

(34) Kresse, G.; Furthmüller, J. Efficiency of ab-initio total energy calculations for metals and semiconductors using a plane-wave basis set. *Comput. Mater. Sci.* **1996**, *6*, 15–50.

(35) Kresse, G.; Furthmüller, J. Efficient iterative schemes for ab initio total-energy calculations using a plane-wave basis set. *Phys. Rev. B: Condens. Matter Mater. Phys.* **1996**, *54*, 11169.

(36) Blöchl, P. E. Projector augmented-wave method. *Phys. Rev. B: Condens. Matter Mater. Phys.* **1994**, *50*, 17953.

(37) Perdew, J. P.; Burke, K.; Ernzerhof, M. Generalized gradient approximation made simple. *Phys. Rev. Lett.* **1996**, *77*, 3865.

(38) Grimme, S.; Antony, J.; Ehrlich, S.; Krieg, H. A consistent and accurate ab initio parametrization of density functional dispersion correction (DFT-D) for the 94 elements H-Pu. *J. Chem. Phys.* **2010**, *132*, 154104.

(39) Grimme, S.; Ehrlich, S.; Goerigk, L. Effect of the damping function in dispersion corrected density functional theory. *J. Comput. Chem.* **2011**, *32*, 1456–1465.

(40) Momma, K.; Izumi, F. VESTA: a three-dimensional visualization system for electronic and structural analysis. *J. Appl. Crystallogr.* **2008**, *41*, 653–658.

(41) Ruiz-Serrano, Á.; Hine, N. D. M.; Skylaris, C.-K. Pulay forces from localized orbitals optimized in situ using a psinc basis set. *J. Chem. Phys.* **2012**, *136*, 234101.

(42) Henkelman, G.; Jónsson, H. Improved tangent estimate in the nudged elastic band method for finding minimum energy paths and saddle points. *J. Chem. Phys.* **2000**, *113*, 9978–9985.

(43) Henkelman, G.; Uberuaga, B. P.; Jónsson, H. A climbing image nudged elastic band method for finding saddle points and minimum energy paths. *J. Chem. Phys.* **2000**, *113*, 9901–9904.

(44) Martyna, G. J.; Klein, M. L.; Tuckerman, M. Nosé-Hoover chains: The canonical ensemble via continuous dynamics. *J. Chem. Phys.* **1992**, *97*, 2635–2643.

(45) Henkelman, G.; Arnaldsson, A.; Jónsson, H. A fast and robust algorithm for Bader decomposition of charge density. *Comput. Mater. Sci.* **2006**, *36*, 354–360.

(46) Liu, W.; Carrasco, J.; Santra, B.; Michaelides, A.; Scheffler, M.; Tkatchenko, A. Benzene adsorbed on metals: Concerted effect of covalency and van der Waals bonding. *Phys. Rev. B: Condens. Matter Mater. Phys.* **2012**, *86*, 245405.

(47) Fang, M.; Liu, X.; Ren, J.-C.; Yang, S.; Su, G.; Fang, Q.; Lai, J.; Li, S.; Liu, W. Revisiting the anchoring behavior in lithium-sulfur batteries: many-body effect on the suppression of shuttle effect. *npj Comput. Mater.* **2020**, *6*, 8.

(48) Manthiram, A.; Fu, Y.; Chung, S.-H.; Zu, C.; Su, Y.-S. Rechargeable Lithium-Sulfur Batteries. *Chem. Rev.* **2014**, *114*, 11751–11787.

(49) Mikhaylik, Y. V.; Kovalev, I.; Schock, R.; Kumaresan, K.; Xu, J.; Affinito, J. High energy rechargeable Li-S cells for EV application: status, remaining problems and solutions. *ECS Trans.* **2010**, *25*, 23.

(50) Fang, Q.; Fang, M.; Liu, X.; Yu, P.; Ren, J.-C.; Li, S.; Liu, W. An asymmetric Ti₂CO/WS₂ heterostructure as a promising anchoring material for lithium-sulfur batteries. *J. Mater. Chem. A* **2020**, *8*, 13770–13775.

(51) Zhang, Q.; Wang, Y.; Seh, Z. W.; Fu, Z.; Zhang, R.; Cui, Y. Understanding the Anchoring Effect of Two-Dimensional Layered Materials for Lithium-Sulfur Batteries. *Nano Lett.* **2015**, *15*, 3780–3786.

(52) Zhao, J.; Yang, Y.; Katiyar, R. S.; Chen, Z. Phosphorene as a promising anchoring material for lithium-sulfur batteries: a computational study. *J. Mater. Chem. A* **2016**, *4*, 6124–6130.

(53) Song, X.; Qu, Y.; Zhao, L.; Zhao, M. Monolayer Fe₃GeX₂ (X = S, Se, and Te) as Highly Efficient Electrocatalysts for Lithium-Sulfur Batteries. *ACS Appl. Mater. Interfaces* **2021**, *13*, 11845–11851.

(54) Tao, X.; Wang, J.; Liu, C.; Wang, H.; Yao, H.; Zheng, G.; Seh, Z. W.; Cai, Q.; Li, W.; Zhou, G.; Zu, C.; Cui, Y. Balancing surface adsorption and diffusion of lithium-polysulfides on nonconductive oxides for lithium-sulfur battery design. *Nat. Commun.* **2016**, *7*, 11203.

(55) Jing, Y.; Zhou, Z.; Cabrera, C. R.; Chen, Z. Metallic VS₂ monolayer: a promising 2D anode material for lithium ion batteries. *J. Phys. Chem. C* **2013**, *117*, 25409–25413.

(56) Zhou, G.; Tian, H.; Jin, Y.; Tao, X.; Liu, B.; Zhang, R.; Seh, Z. W.; Zhuo, D.; Liu, Y.; Sun, J.; Zhao, J.; Zu, C.; Wu, D. S.; Zhang, Q.; Cui, Y. Catalytic oxidation of Li₂S on the surface of metal sulfides for Li-S batteries. *Proc. Natl. Acad. Sci.* **2017**, *114*, 840–845.